JKAU: Sci., **Vol. 34**, No. 2, pp: 65 - 77 (2024)
DOI:10.4197/Sci.34-2.5

Optimizing Continuous Wave Semiconductor Laser toward Achieving (100's) mW Power for Use in Medical Application: Theoretical Work

Fatima AL-Shaikh, Abubakr El-Zarrad and **Moustafa Ahmed**

Department of Physics, Faculty of Science, King Abdulaziz University, Jeddah, Saudi Arabia

falishaikhmohamed@stu.kau.edu.sa

Abstract. Diode laser is very efficient in medical applications, especially in photodynamic therapy (PDT), a type of laser phototherapy. Conventional laser diodes are classified as low-power lasers emitting radiation with a power of 10s-mW. Extending the laser diode to further applications requires enhancing the radiated power. In this theoretical research, we aim to optimize the laser diode's continuous-wave (CW) parameters that control the light-current (L-I) characteristics toward achieving higher slope efficiency and output power. The study is based on a numerical solution of the rate equations and evaluation of the steady state value of the emitted power, which is then used in the relationships among the total slope efficiency, differential quantum efficiency, threshold current, and emitted power. The numerical calculations indicated that power in the range of 100s-mW is predicted by designing the laser to a short cavity with an anti-reflecting front facet (~1%), a high-reflecting back facet (~99%), lower internal loss ($100m^{-1}$), and large optical confinement (30%). Therefore, the outcome of this study is to offer a guide for designing a high-power laser diode for use in PDT.

Keywords: Laser diode, Laser photodynamic therapy, Efficiency, Light-current curve.

1. Introduction

In the twentieth century, lasers were one of the most important inventions. They have found numerous uses in daily life and industry. They are found in reading bar codes, compact discs, laser pointers for position and motion control, computer printers and mouse, holography, optical communications, and processing of material. Lasers are also used in chemistry and spectroscopy to identify materials. High-power lasers can be used to cut metal and in military systems [1]. Further, in medical applications, lasers are faster and less invasive and are highly precise, therefore they have penetrated most medical disciplines, like ophthalmology, dermatology, dentistry, otolaryngology, urology, gastroenterology, cardiology, gynecology, neurosurgery and orthopedics [2]. Many diseases are now treated and diagnosed with the aid of lasers. One excellent illustration of how a movement can improve healthcare is medical lasers [2]. Among all the types of lasers used in medical applications, the semiconductor laser has several advantages, including the ability to be pumped directly by an electrical current, its high efficiency, its long lifetime, its small size, its ease of connection to optical fibers, and its low cost, its light can be generated in a wide spectrum range; it is tunable [3, 4,5].

A common use of lasers in medicine is photodynamic treatment (PDT), in which laser radiation and biological tissue interact with each other through a process known as photochemistry [2]. Precancerous lesions and superficial tumors are frequently treated with PDT. Three components work together to selectively destroy the target tumor in photodynamic therapy (PDT): light with a certain wavelength, molecules of oxygen, and compounds known as photosensitizers (PS). Since PDT is a non-invasive, non-thermal, and non-ionized (or non-toxic) cancer treatment, it can be repeated. Additionally, because the type of tumor determines which type of photosensitizer to utilize, PDT has a high degree of tumor selectivity [6-8]. Since

lasers can be attached to optical fibers to reach remote positions and reduce the scatter of light, they are preferred in PDT. They produce high intensity coherent monochromatic collimated light with a forward scattering behavior, which leads to a tissue penetration depth higher than non-coherent light [6-9]. Four types of lasers can be employed in PDT: semiconductor lasers, solid-state lasers like Nd: YAG lasers, metal vapor pumped lasers like copper vapor lasers, and argon pumped lasers. The complicated, large, and costly laser systems of the past have been replaced by the affordable, dependable, compact, and easy-to-use laser diode [6].

Because of their extensive use as solid-state laser pumps and their vast range of direct applications, semiconductor lasers rank among the most significant groups of lasers in use today[10]. A direct bandgap semiconductor serves as the gain medium in semiconductor lasers. A Fabry-Perot (FP) cavity made of cleaved facets is used to get optical feedback, and dielectric waveguiding is used to accomplish mode confinement. In order to pump energy, current is injected into the active area. A photon that has energy equal to the band gap energy can be released by an excited electron in a semiconductor when it recombines with a positive charge (hole) in the valence band. At a wavelength of 805 nm, AlGaAs diodes are commonly found in commercial products. Obtainable wavelengths range from ultraviolet to infrared. When the optical gain in the laser cavity balances the cavity losses, which include the internal loss and losses at the facet mirrors, the lasing process begins [2,11]. The gain, which regulates the laser output's power and spectrum distribution, is no longer a linear function of the injected carrier density over the threshold level. Rather, intraband relaxation processes of the charge carriers [12], which cause spectral-hole burning and carrier heating [13], clamp or suppress gain below the threshold gain. A semiconductor laser's dynamics and light-output (L-I) properties are ascertained by solving a system of rate equations that take into account all of the mechanisms by which photons and carriers are added to or discarded from the active area. Important components that are incorporated in the rate equations include the cavity photon density, photon lifetime, gain coefficient, gain suppression, and confinement of the oscillating modes into the active region field [13].

The poor light penetration depth through the tissue is PDT's main problem [6,8,14-17]. Due to this restriction, PDT can only be used to treat superficial lesions; deeper tumors must be treated with an interstitial PDT [14]. As a result, a powerful laser beam is needed for the effective use of PDT [17,18]. According to Lim, the PDT laser system's output varies from 10 to 300 mW based on the duration of exposure[19]. The range of 50–150 mW for laser's power was reported by Fuchs et al.[17] as power increases, so does penetration depth. To increase the penetration depth in tissues, PDT requires the effective employment of semiconductor lasers that emit in the CW mode at a power of 100s-mW. CW laser diodes of various strengths are used in numerous PDT preclinical research, including *in vitro* [20-23] and *in vivo* [24-26]. The output power in each of these studies falls between 40 and 300 mW.

In general, laser diodes are categorized as low-power lasers since they only produce light with a few 10s-mW of power. Increasing the output power to 100s-mW or even the watt-class is necessary to expand the use of the laser diode. Asymmetric heterostructures with an ultrawide waveguide[27], asymmetric separate confinement heterostructure (SCH) multiple-quantum-well lasers[28], erbium-doped fiber amplifiers (EDFAs)[29], and fiber-couples laser diodes [30] are examples of special structures that have been used to increase laser power.

The task of reaching 100 milliwatts of output power necessitates improving the overall slope efficiency of the L-I characteristics, which is contingent upon the gain medium and structure parameters. This work aims to theoretically provide a guide for designing a semiconductor laser with a conventional, cost-effective structure that can emit CW with a power of 100 mW for use in PDT. This will help overcome the limited penetration depth and improve the deep-level therapeutic effect of the cancer treatment. We seek for parameters that govern

the (L-I) characteristics and give a basic theoretical examination of the laser diode power. The study's methodology involves solving the rate equations numerically, calculating the emission power's steady state value, and applying that value to the relationships between the emission power, threshold current, differential quantum efficiency, and slope efficiency. We demonstrate that the use of an anti-reflecting front facet, a high-reflecting back facet, and a cavity with short length and with good optical confinement and low internal loss may forecast powers in the range of 100s-mW.

2. Modeling of CW Laser Output

The static and dynamic characteristics of laser diodes are commonly simulated by solving the standard rate equations which represent time transformation of photons number $S(t)$ and carriers number $N(t)$ injected into the laser cavity. At a given injection current (I), these rate equations are given in terms of the laser parameters as[31]:

$$\frac{dS}{dt} = \Gamma G(N,S)S - \frac{S}{\tau_P} + \beta_{sp}\frac{N}{\tau_e} \tag{1}$$

$$\frac{dN}{dt} = \frac{I}{e} - \frac{N}{\tau_e} - G(N,S)S \tag{2}$$

where $G(N,S)$ is the optical gain coefficient and is expressed by nonlinear form as the following:

$$G(N,S) = \frac{\frac{g_0}{V}(N-N_g)}{1+\epsilon S} \tag{3}$$

Laser parameters contained in the above equations are defined as follows:

Γ: confinement factor of the mode energy contained in the active region

g_0: slope of a linear relation of linear gain versus carrier number, or tangential gain

V: active region volume

N_g: number of electrons at transparency

ϵ: coefficient of gain suppression

τ_P: lifetime of photon

β_{sp}: factor of spontaneous emission

τ_e: lifetime of electron due to spontaneous emission

e: charge of electron

In the rate equation of photon eq. (1), the first term ΓGS is the rate of increase the photon density due to stimulated emission. The confinement factor Γ accounts for the gain reduction that occurs because of the spreading of the optical mode beyond the active region. While the second term is the rate of photons that lost in the cavity, including the internal and mirrors loss, manifested as the photon decay time constant (τ_P), the third term is the spontaneous emission contribution from the carrier radiative recombination into the laser mode. On the other hand, the first term on the right side of the rate equation of carrier eq. (2) is the injected carrier rate (I/e), the second term is the rate of carrier depletion due to all processes of recombination (expressed by the electron decay time (τ_e)) and the third term is the carrier reduction because of stimulated emission, which is proportional to the photon density and medium gain.

The Eqs. (1) and (2) can be solved numerically. In this case, the solution reveals the laser transients in which the laser shoes relaxation oscillations followed by a steady state in which

the number of photons (S) and carriers (N) remain constant, S_0 and N_0, respectively. The front facet emitted power (P_f) in terms of the number of photons is given as

$$P_f = \frac{(1-R_f)\sqrt{R_b}}{(\sqrt{R_f}+\sqrt{R_b})(1-\sqrt{R_f R_b})} v_g \alpha_m h\upsilon S_0 \tag{4}$$

where

$$\alpha_m = \frac{1}{2L} ln\left(\frac{1}{R_f R_b}\right) \tag{5}$$

is the mirror loss and describe the radiation escaping from cavity because of finite facet reflectivities R_f and R_b at the front and back facets, respectively, and L is the length of the active region. The combination of mirror loss α_m and internal loss α_i induced by free-carrier absorption, scattering, and other possible mechanisms, such as Auger recombination, defines the laser gain at threshold

$$G_{th} = \frac{1}{\tau_p} = v_g(\alpha_i + \alpha_m) \tag{6}$$

where τ_p is the lifetime of photon, and $v_g = c/n$ is the group velocity, n is the effective refractive index and c is the light speed in free space. The threshold current (I_{th}) is determined from the level of G_{th} as

$$I_{th} = \frac{eN_{th}}{\tau_e} = \frac{e}{\tau_e}\left(N_g + \frac{1}{\tau_p \Gamma g_0}\right) = \frac{e}{\tau_e}\left(N_g + \frac{v_g(\alpha_i+\alpha_m)}{\Gamma g_0}\right) \tag{7}$$

where the approximation of Eq. (3), $G_{th} \approx \frac{g_0}{V}\left(N_{th} - N_g\right)$ was used. At current injections far beyond the threshold level (I_{th}), the power value (P_f) at a given current (I) can be approximated as[31]:

$$P_f = \frac{h\upsilon}{e}\eta_d (I - I_{th}) \tag{8}$$

where

$$\eta_d = \frac{rate\ of\ photon\ escape\ out\ of\ cavity\ (v_g\alpha_m)}{rate\ of\ photon\ generation\ (1/\tau_p)} = \eta_i \frac{\alpha_m}{\alpha_i+\alpha_m} \tag{9}$$

is the laser differential quantum efficiency, h is the constant of Planck, υ is the frequency of laser output, and I_{th} is the value of current at threshold.

Equation (8) describes the linear part of the so-called "light versus current (L-I) characteristics" of the laser in which the stimulated emission takes over the laser output. The L-I curve is an important characteristic of any laser diode, because it determines the amount of emitted power at a given injection level. The slope of this linear curve is called the total slope efficiency (S_{tot})

$$S_{tot} = \frac{h\upsilon}{e}\eta_d = \left(\frac{h\upsilon}{e}\right)\eta_i\left(\frac{\alpha_m}{\alpha_i+\alpha_m}\right) \tag{10}$$

where η_i is the internal quantum efficiency, it describes the number of photons generated inside the cavity for each injected carrier[32]. For most semiconductor lasers, η_i is almost 100%.

3. Methodology of Increase Laser Power

The Eqs. (1) and (2) are numerically solved by the 4th order Runge-Kutta algorithm. and the steady state values S_0 and N_0 of S and N are evaluated.

Equation (8) indicates that to increase the emitted power P_f, it is required to (1) increase the differential quantum efficiency η_d and consequently the slope efficiency S_{tot}, and/or (2) increase the injection level I far beyond the threshold current I_{th}.

As indicated in equation (9), for lasers emitting at wavelength of 1μm, the value of hυ/e is 1.246 mW/mA which represents the maximum value of S_{tot} because $\eta_i \leq 100\%$, and $\frac{\alpha_m}{\alpha_i+\alpha_m} < 1$. Thus, the increase in the S_{tot} value is related to increase the mirror loss α_m and/or decrease the internal loss α_i. If the loss is too high, photons will escape from the laser cavity too quickly and will not be sufficiently amplified. However, if the loss is too low, most photons will circulate within the cavity rather than being emitted as output. Therefore, reasonably increasing the mirror loss can help find the optimal balance between gain and output power. Referring to equation (5), the increase in mirror loss α_m is produced by reducing the active region length L and/ or reducing the facet reflectivities product R_fR_b. The latter can be achieved by using an anti-reflecting coating on the front facet, R_1~0.01, while the back facet reflectivity can be designed with conventional reflectivity, R_2~0.33.

On the other hand, reducing the threshold current I_{th} requires reducing both mirror loss α_m and internal loss α_i, and increasing the confinement factor Γ for the same amplifying semiconductor material.

In the following section, we present results on increasing the slope efficiency S_{tot} and reducing the threshold current I_{th}as well as results on the L-I characteristics for >100 mW laser diodes proposed to medical applications.

4. Results and Discussions

4.1 Slope Efficiency

The slope efficiency S_{tot} is describes as a growing ratio in light intensity or output power ΔP to the growing in input injection current ΔI. We seek the optimum parameters values that match to high values of slope efficiency S_{tot}. We studied the effect of the length (L), internal loss (α_i) and back facet reflectivity (R_b). Table 1 lists the numerical values of the InGaAs laser's parameters utilized in computations.

Table 1. Fortran program's input parameters of 1μm-InGaAs laser.

Symbol	Meaning	Value
d	Thickness	0.1 μm
w	Width	5 μm
η_i	Quantum efficiency	100%
λ	Wavelength	1 μm
v_g	Group velocity	$8.5x10^7$ m/s
g_0	Gain coefficient	$2.5\ x10^{-20}$ m^2
Γ	Confinement factor	0.2
τ_e	Spontaneous emission factor	1 ns
N_g	Carrier density	$1x10^{24}$ m^{-3}

Figures 1(a) and (b) plot variation of S_{tot} with length L (100~600 μm) at different levels of internal loss α_i (100, 500 and 1000 m^{-1}) when using R_f = 0.01, R_b = 0.99, and at different values of R_f using R_b = 0.99 and α_i =100 m^{-1}, respectively. Figure 1(a) shows that at each value of α_i, S_{tot} is reduced almost linearly with the increase of length L, and the slope of this reduction increases with the increase of α_i. At a specific layer length L, S_{tot} is enhanced by reducing the internal loss α_i. The maximum value is then obtained at the smallest values of both L and α_i.In the same manner, Fig. 1(b) shows that at each value of R_f, S_{tot} is slightly reduced with the

increase of length L. At a specific layer length L, S_{tot} is enhanced with reducing facet reflectivity R_f, and the maximum value is then obtained at the smallest values of both L and R_f.

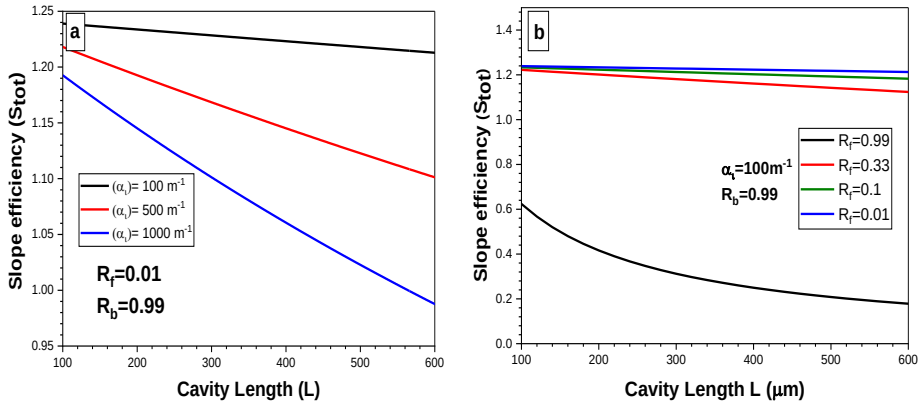

Fig. 1. Effect of cavity length (L) on slope efficiency (Stot): (a) at different values of α_i with Rfand Rb kept constant, and (b) at different values of Rf with α_i and Rb kept constant.

4.2 Threshold Current

It is obvious from equation (7) that reducing the threshold current I_{th} for the same amplifying semiconductor could be achieved by reducing both mirror loss $\alpha_m$and internal loss α_i, and increasing the confinement factor Γ. In Fig. 2(a) and (b), we plot the values of I_{th} that correspond to the results of the slope efficiency S_{tot} in Fig. 1(a) and (b), respectively. Figure 2(a) shows that when R_f = 0.01, R_b = 0.99, I_{th} increases linearly with the increase of length L for the three relevant values of internal loss α_i, and the slope of variation increases with the increase of α_i. The lowest values of I_{th} are around 0.047A and are obtained for the shortest length of L = 100μm. On the other hand, Fig. 2(b) that corresponds to R_b = 0.99 and α_i= 100 m^{-1} shows that the threshold current I_{th} could be reduced further to less than 0.02A by designing a front facet with higher reflectivity R_f. However, the latter choice may correspond to lower output power. Nevertheless, we will study below influence of these parameters on the L-I characteristics and examine the amount of power emitted.

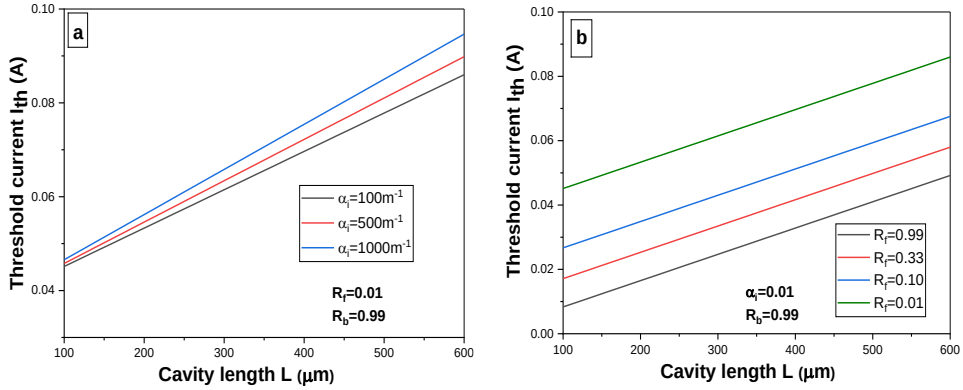

Fig. 2. Effect of cavity length (L) on threshold current (I_{th}): (a) at different values of (α_i) with Rf and Rb kept constant, and (b) at different values of Rf with (α_i) and Rb kept constant.

The reduction of threshold current I_{th} with the rise of the confinement factor Γ is illustrated in Fig. 3 for parameters yielding maximum slope efficiency S_{tot} (R_f=0.01, R_b=0.99, α_i=100m^{-1} and L=100μm). The figure shows that I_{th} drops from 0.16 A to 0.03 A with the increase of Γ from 0.05 to 0.4.

4.3 Light-Current (L-I) Characteristics

In this work, we examined how the parameters controlling the laser's output power P_f; namely, L, R_b, α_i and Γ, on the characteristics of L-I curve of the laser diode under investigation.

We aim to find the optimum values of these parameters that correspond to power levels exceeding 100mW.

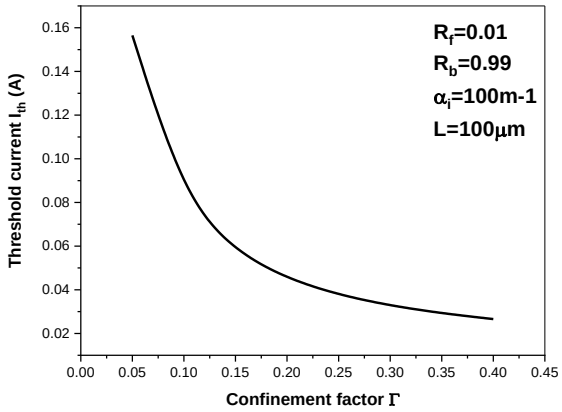

Fig. 3. Variation of I_{th} with the confinement factor Γ when Rf=0.01, Rb=0.99, α_i=100m^{-1} and L=100µm.

The characteristics of a semiconductor laser's emission are characterized by the (L–I) curve, which shows both the threshold level and the current required to achieve a certain power output. Figure 4(a) plots the L-I characteristics for three cavity lengths of L = 100, 300 and 500µm, when the other parameters are set to be R_f=0.01, R_b=0.33, α_i = 100m^{-1} and Γ =0.2. The figure reveals that the slope of the linear relation between P_f and I decrease with the increase of length L, whereas the intercept with the current axis, or the threshold current I_{th}, increases with the increase of L. These outcomes are in line with those of Fig. 1(a) and 2(a). Under these conditions, the power reaches P_f=150mW when I=73.5, 76 and 78.5mA when L = 100, 300 and 500µm, respectively. On the other hand, we plot variations of the L-I characteristics with the internal loss α_i when R_f=0.01, R_b=0.33, L=100µm and Γ =0.2 in Fig. 4(b). The figure indicates small reduction of the slope S_{tot} with the increase of α_i, while the threshold current is subject to minor changes, as indicated in Fig. 1(a) and 2(a).

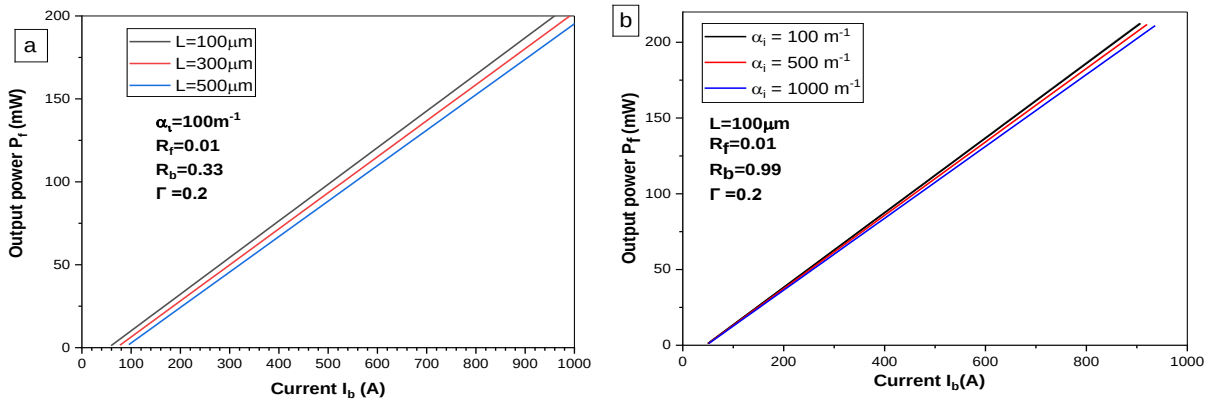

Fig. 4. L-I curve under (a) different cavity lengths, and (b) different internal loss, when Rf=0.01, Rb=0.33, α_i=100m^{-1} and Γ =0.2.

The L-I curve is temperature dependent and the laser performance degrades at high temperatures, where a part of the overall current may not flow through the active region in the form of a leakage current. So, Eq. (8) would be modified to:

$$P_f = \frac{h\upsilon}{e}\eta_d(I - I_{th} - \Delta I_L)$$

where ΔI_L represents the possible growth in the leakage current with the current I. The greatest power that these lasers can produce when operating in (CW) at room temperature is constrained by a thermal runaway process, which causes an increase in internal temperature as extra current

is needed to counteract the influence of the rising temperature. As a result, using a built-in thermoelectric cooler to regulate their temperature is frequently essential. The L-I curve's slope efficiency is not always constant in practice, and for large values of I, the output power saturates. This might occur as a result of an increase in leakage current with I, which would reduce the amount of device current that injects carriers into the active layer. One potential explanation could be junction heating, which could lead to a decrease in the time of carrier recombination τ_e as the laser power rises. One possible explanation for the decline in τ_e could be Auger recombination, which rises sharply with temperature. Throughout the 1990s[33-35], Distributed Feedback (DFB) lasers saw significant improvements in their thermal performance[33-35]. For instance, utilizing a strained Multi-Quantum Well (MQW) architecture, DFB lasers with power outputs more than 100 mW at ambient temperature were created [36]. This paper is not intended to study these thermal impacts on the L-I characteristics; a comprehensive description of the gain and loss dependence on temperature is needed. The current model seems adequate as long as the current stays below the saturation limit and as long as we are searching for assistance to help optimize the laser parameters in order to achieve high power emission, despite the major impact of these thermal effects. Future research will look at how this investigation's findings were impacted by temperature.

In Fig. 5, we examine the influence of the power reflectivity R_b on the L-I characteristics of the laser, while keeping the power reflectivity at the front facet at R_f=0.01. As shown in the figure, the slope S_{tot} improves, and the threshold current I_{th} decreases with increasing the reflectivity R_b from 0.33 to 0.99. This effect manifests as reducing the current required to achieve power of P_f=200mW from 0.96 to 0.86A with the increase of reflectivity R_2 from 0.33 to 0.99. In other words, applying an anti-reflection coating to the front facet lowers its reflectivity, while applying a high-reflection coating to the back facet increases the output power from the facet.

Also, injection level of, for example, I = 0.7A results in emitted power of P_f=141 and 160mW when R_2 increases from 0.33 and 0.99 respectively.

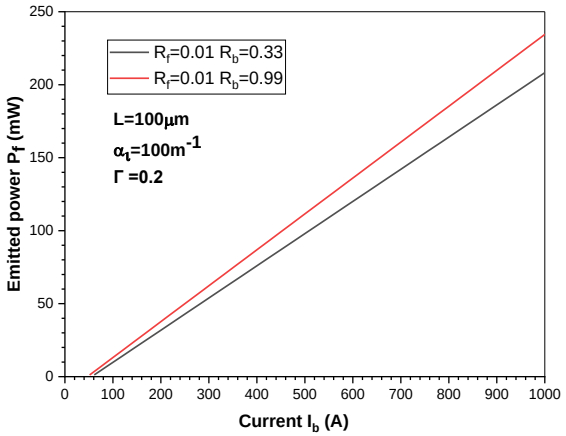

Fig. 5. Influence of the power reflectivity Rb at the back facet on the L-I characteristics of the laser, while keeping the Rf=0.01. Other parameters are set to be L=100µm, α_i = 100m^{-1} and Γ =0.2

The influence of the confinement factor Γ on the L-I characteristics is plotted in Fig. 6 when the laser parameters are kept at R_f=0.01, R_b=0.99, L=100µm and α_i= 100m^{-1}. It is interesting to notice that the increase in the value of Γ results in a dramatic increase in the slope S_{tot} associated with noticeable reduction of the threshold current I_{th}. Although the slope efficiency S_{tot} does not depend explicitly on Γ as seen in equation (10), the shown variation originates from the calculations of the power P_f via the original equation (4) rather than the approximated one (8). The figure indicates that a power level of P_f=300mW is predicted at a

current level of I=845mA when Γ =0.3, while this current results in power of P_f=195 and 92mW when Γ decreases to 0.2 and 0.1, respectively.

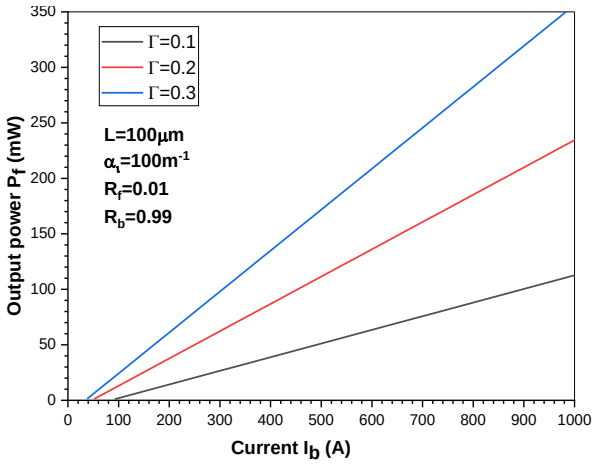

Fig. 6. Influence of the confinement factor Γ on the L-I characteristics of the laser. The parameters of the laser are set to be Rf=0.01, Rb=0.99, L=100μm and α_i = 100m^{-1}.

The above analysis indicated that the optimum values of the parameters that yield output power in the range of P_f=100~300mW are R_f as low as 0.01, R_b as high as 0.99, L as short as 100μm, α_i as small as 100m^{-1}, and $\Gamma > 0.2$. It is then interesting to compare the L-I characteristics predicted by these optimum parameters with those of the laser when using the corresponding conventional values of these parameters. The comparison is plotted in Fig.7, which exhibits dramatic improvement in the slope efficiency S_{tot} from 96.6 to 368.9 mW/mA and reduction of the threshold current I_{th} from 52 to 36 mA. The maximum achievable power for the conventional laser is 90mW when the current is 1A, however, this power rises to 360mW for the optimum laser.

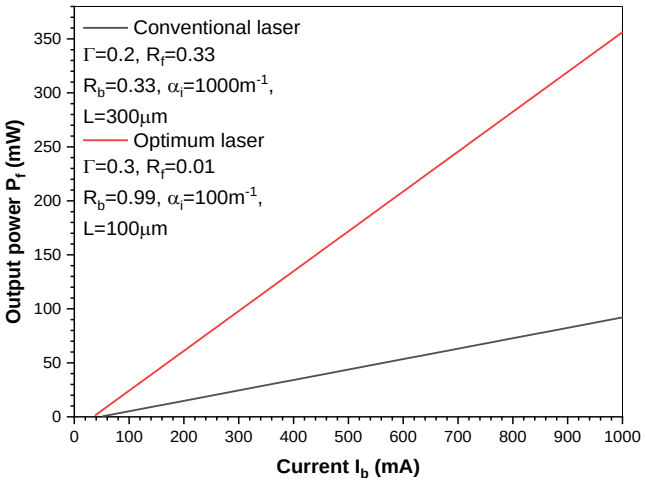

Fig. 7. L-I curves of both the optimized laser and conventional laser of 1-μm InGaAs laser diodes.

High-power 635–690 nm laser diodes are frequently utilized in PDT. It is worthwhile to demonstrate how the current model is used to forecast the optimum L-I properties of these lasers. We apply the following values of the InGaN laser parameters. g_0 = 1.62x10^{-20} m^2, N_g = 1.43 x 10^{25} m^{-3}, v_g = 1.14x10^8 m/s, τ_e = 2 ns, ϵ =1.9x10^{-23} and λ=650 nm [37,38]. Plotting the L-I characteristics with optimum parameters (R_f=0.01, R_b=0.99, L=120μm, α_i=100m^{-1}, and Γ=0.3) for both the conventional semiconductor laser and the laser is shown in Fig. 8. The graph shows that the slope efficiency increased from 753 mA to 1904 mW/mA, while the threshold current decreased from I_{th} = 200 mA to 80 mA. This slope efficiency value is considerably greater than the InGaAs laser value in Fig. 7. As revealed in both figures, the InGaN laser has an output

power of 610 mW at currents of I = 1A, which is greater than the AlGaAs laser's 90 mW equivalent power.

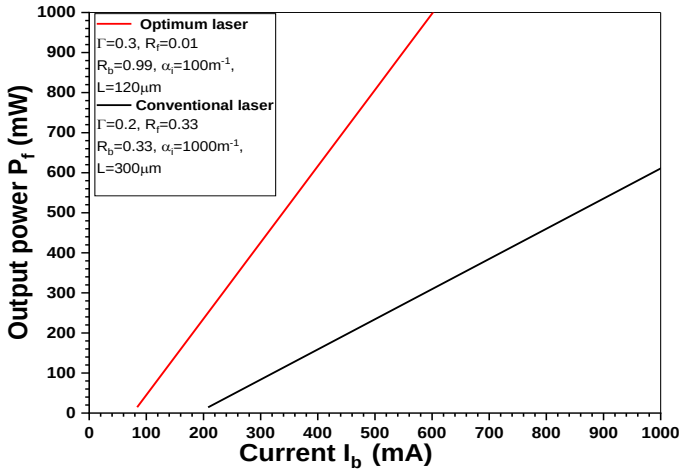

Fig. 8. L-I curves of both the optimized laser and conventional laser of 650-nm InGaN laser diodes.

For practical implications of facet reflectivities and internal loss parameters, Kasukawa et al. reported achieving output power as high as 360 mW from the front facet of a 1480-nm laser diode for EDFA pumping using front-facet reflectivity of 5% and back-facet reflectivity of 95%[29]. The internal loss was reduced effectively by introducing a quantum-well structure, which assisted to provide low threshold current and high differential quantum efficiency operation. Furthermore, seeking a laser diode with output power reaching 2W for use in material processing and pumping lasers, Gai et al.[39] reduced the internal loss to 0.8 cm^{-1} by designing an asymmetric broad waveguide structure based on the fact that the optical absorption in n-type semiconductor materials is lower than that in p-type semiconductor materials[40]. The laser diodes were designed with 5% anti-refection coating on the front facet and 95% high-refection coating on the rear. Such asymmetric structure provides effective carrier confinement.

It is worth mentioning that the characteristics of the semiconductor laser are affected by gain suppression which appears in Eq. (3) as $(1 + \epsilon S)^{-1}$, that describes the gain suppression at high powers. Usually, this gain suppression is less than 1 % and has a slight impact on the L-I characteristics. The inclusion of this gain suppression into the rate equations is important and useful to describe the dynamics of the laser, such as modulation and noise [31,41-44]. Although the physical processes that contribute to gain nonlinearities are not completely understood, it has been shown that carrier heating, two-photon absorption, and spatial and spectral hole burning are phenomena responsible for nonlinear gain[45,46].

5. Conclusions

We determined on scaling the laser design parameters that yield power emitted in the range of hundreds milliwatt for applied in medical applications, such as photodynamic therapy. The optimum evaluation of these parameters includes values of the front facet reflectivity as low as 0.01, and the back facet reflectivity as high as 0.99, length of cavity as short as 100μm, internal loss as small as 100m^{-1}, and confinement factor greater than 0.2. These parameters were discovered to reduce the threshold current and optimize the laser's total slope efficiency.

Conflict of Interest

The authors declare that they have no financial interests/personal relationships which may be considered as potential competing interests.

Data Availability

The datasets generated during and/or analyzed during the current study are available from the corresponding author on reasonable request.

References

[1] Jain VK. *Laser Systems and Applications*. Alpha Science Internation Limited; 2013.

[2] Peng Q, Juzeniene A, Chen J, et al. Lasers in medicine. *Reports on Progress in Physics*. 2008/04/11 2008;71(5):056701. doi:10.1088/0034-4885/71/5/056701

[3] Hulicius E, Kubeček V. 8 - Semiconductor lasers for medical applications. In: Jelínková H, ed. *Lasers for Medical Applications*. Woodhead Publishing; 2013:222-250.

[4] Dörschel K, Müller G, Schaldach B, et al. Basic Physics of Lasers. In: Berlien HP, Müller GJ, eds. *Applied Laser Medicine*. Springer Berlin Heidelberg; 2003:9-71.

[5] H.-Peter B. *Applied Laser Medicine*. Springer-Verlag Berlin Heidelberg; 2003.

[6] Rodrigues JA, Correia JH. Enhanced Photodynamic Therapy: A Review of Combined Energy Sources. *Cells*. 2022;11(24). doi:10.3390/cells11243995

[7] Roggan A, Bindig U, Wäsche W, et al. Action Mechanisms of Laser Radiation in Biological Tissues. In: Berlien HP, Müller GJ, eds. *Applied Laser Medicine*. Springer Berlin Heidelberg; 2003:73-127.

[8] Yoon I, Li JZ, Shim YK. Advance in photosensitizers and light delivery for photodynamic therapy. *Clin Endosc*. Jan 2013;46(1):7-23. doi:10.5946/ce.2013.46.1.7

[9] Mallidi S, Anbil S, Bulin AL, Obaid G, Ichikawa M, Hasan T. Beyond the Barriers of Light Penetration: Strategies, Perspectives and Possibilities for Photodynamic Therapy. *Theranostics*. 2016;6(13):2458-2487. doi:10.7150/thno.16183

[10] Svelto O. Solid-State, Dye, and Semiconductor Lasers. In: Svelto O, ed. *Principles of Lasers*. Springer US; 2010:375-430.

[11] Agrawal GP, Dutta NK. Introduction. In: Agrawal GP, Dutta NK, eds. *Semiconductor Lasers*. Springer US; 1993:1-24.

[12] Ahmed M, Yamada M. An infinite order perturbation approach to gain calculation in injection semiconductor lasers. *Journal of Applied Physics*. 1998;84(6):3004-3015. doi:10.1063/1.368453

[13] Chin-Yi T, Fang-Ping S, Tien-Li S, Tsu-Yin W, Chih-Hsiung C, Chin-Yao T. A small-signal analysis of the modulation response of high-speed quantum-well lasers: effects of spectral hole burning, carrier heating, and carrier diffusion-capture-escape. *IEEE Journal of Quantum Electronics*. 1997;33(11):2084-2096. doi:10.1109/3.641324

[14] Jamil B, Berlien HP. Basics of Photodynamic Therapy (PDT). In: Berlien HP, Müller GJ, eds. *Applied Laser Medicine*. Springer Berlin Heidelberg; 2003:251-288.

[15] Algorri JF, Ochoa M, Roldán-Varona P, Rodríguez-Cobo L, López-Higuera JM. Light Technology for Efficient and Effective Photodynamic Therapy: A Critical Review. *Cancers*. 2021;13(14). doi:10.3390/cancers13143484

[16] Algorri JF, López-Higuera JM, Rodríguez-Cobo L, Cobo A. Advanced Light Source Technologies for Photodynamic Therapy of Skin Cancer Lesions. *Pharmaceutics*. 2023;15(8). doi:10.3390/pharmaceutics15082075

[17] Fuchs B, Berlien HP, Philipp CM. Therapeutic Guidelines. In: Berlien HP, Müller GJ, eds. *Applied Laser Medicine*. Springer Berlin Heidelberg; 2003:211-234.

[18] Hamdy O, Mohammed HS. Variations in tissue optical parameters with the incident power of an infrared laser. *PLoS One*. 2022;17(1):e0263164. doi:10.1371/journal.pone.0263164

[19] Lim HS. Development and optimization of a diode laser for photodynamic therapy. *Laser Ther*. 2011;20(3):195-203. doi:10.5978/islsm.20.195

[20] Etemadi A, Azizi A, Pourhajibagher M, Chiniforush N. *In Vitro* Efficacy of Antimicrobial Photodynamic Therapy With Phycocyanin and Diode Laser for the Reduction of Porphyromonas gingivalis. Article. *Journal of Lasers in Medical Sciences*. 2022;13:1-7. doi:10.34172/jlms.2022.55

[21] Astuti SD. An *in vitro* antimicrobial effect of 405 nm laser diode combined with chlorophylls of Alfalfa (Medicago sativa L.) on Enterococcus faecalis. Article. *Dental Journal: Majalah Kedokteran Gigi*. 03// 2018;51(1):47-51. doi:10.20473/j.djmkg.v51.i1.p47-51

[22] Mohammed MG, Maki AM. Effect of 410 nm Diode Laser Irradiation on the Growth of Burn Wounds-associated Bacteria, Pseudomonas Aeruginosa and Staphylococcus Aureus. Article. تأثير أشعة ليزر الدايود ٤١٠ نانومتر على نمو بكتريا *Pseudomonas aeruginosa* و *Staphylococcus aureus* المرتبطة بجروح الحروق. ٢٠١٧؛١٦(٢):١١-١٩.

[23] Parasuraman P, Antony AP, B SLS, et al. Antimicrobial photodynamic activity of toluidine blue encapsulated in mesoporous silica nanoparticles against Pseudomonas aeruginosa and Staphylococcus aureus. *Biofouling*. 2019/01/02 2019;35(1):89-103. doi:10.1080/08927014.2019.1570501

[24] Motamedifar M, Tanideh N, Mardani M, Daneshvar B, Hadadi M. Photodynamic antimicrobial chemotherapy using indocyanine green in experimentally induced intraoral ulcers in rats. *PHOTODERMATOLOGY PHOTOIMMUNOLOGY & PHOTOMEDICINE*. MAR 2021;37(2):115-122. doi:10.1111/phpp.12618

[25] Andisheh-Tadbir A, Yaghoubi A, Tanideh N, Mardani M. The effect of indocyanine green-mediated photodynamic therapy in healing of experimentally induced oral mucosal traumatic ulcer in rat. *LASERS IN MEDICAL SCIENCE*. APR 2021;36(3):611-618. doi:10.1007/s10103-020-03096-x

[26] Tenore G, Palaia G, Migliau G, et al. Evaluation of Photodynamic Therapy Using a Diode Laser 635 nm as an Adjunct to Conventional Chemo-Mechanical Endodontic Procedures against Enterococcus faecalis Biofilm: Ex-Vivo Study. *APPLIED SCIENCES-BASEL*. FEB 2020;10(8)2925. doi:10.3390/app10082925

[27] Bezotosnyĭ VV, Vasil'eva VV, Vinokurov DA, et al. High-power laser diodes of wavelength 808 nm based on various types of asymmetric heterostructures with an ultrawide waveguide. Article. *Semiconductors*. 2008;42(3):350-353. doi:10.1007/s11453-008-3020-7

[28] Chen W, Li L, Zhao J, et al. 1.47 μm high characteristic temperature InGaAsP/InP MQW laser. 2012:115-118.

[29] Kasukawa A, Mukaihara T, Yamaguchi T, Kikawa J. Recent Progress of High Power Semiconductor Lasers for EDFA Pumping. *Furukawa Review*. 01/01 2000;

[30] Li Z, Li T, Lu P, et al. A survey of the high power high brightness fiber coupled laser diode. 2012:52-55.

[31] Agrawal GP, Dutta NK. Rate Equations and Operating Characteristics. In: Agrawal GP, Dutta NK, eds. *Semiconductor Lasers*. Springer US; 1993:231-318.

[32] Agrawal GP, Dutta NK. Basic Concepts. In: Agrawal GP, Dutta NK, eds. *Semiconductor Lasers*. Springer US; 1993:25-73.

[33] Bayvel P. Distributed feedback semiconductor lasers John Carroll, James Whiteway and Dick Plumb. *Optical and Quantum Electronics*. 1999/03/01 1999;31(3):291-292. doi:10.1023/A:1006945920291

[34] Ghafouri-Shiraz H, Lo BSK. *Distributed Feedback Laser Diodes: Principles and Physical Modelling*. Wiley; 1996.

[35] Morthier G, Vankwikelberge P. *Handbook of Distributed Feedback Laser Diodes*. Artech House optoelectronics library. Artech House; 1997.

[36] Chen TR, Ungar J, Iannelli J, Oh S, Luong H, Bar-Chaim N. High power operation of InGaAsP/InP multiquantum well DFB lasers at 1.55 μm wavelength. *Electronics Letters*. Institution of Engineering and Technology; 1996;32(10):898-898. https://digital-library.theiet.org/content/journals/10.1049/el_19960601

[37] Ahmed M. Theoretical modeling of intensity noise in InGaN semiconductor lasers. *ScientificWorldJournal*. 2014;2014:475423. doi:10.1155/2014/475423

[38] Tronciu VZ, Yamada M, Ohno T, Ito S, Kawakami T, Taneya M. Analysis of self-pulsation characteristics of InGaN laser diode. *physica status solidi (c)*. 2003/12/01 2003;n/a(7):2296-2299. doi:https://doi.org/10.1002/pssc.200303377

[39] Gai K, Li L, Zhao J, et al. *The simulation analysis of GaInAsP/GaInP diode lasers emitting at 808 nm*. 2012:138-141.

[40] Hayakawa T, Wada M, Yamanaka F, et al. Effects of broad-waveguide structure in 0.8 μm high-power InGaAsP/InGaP/AlGaAs lasers. *Applied Physics Letters*. 1999;75(13):1839-1841. doi:10.1063/1.124845

[41] Dynamic Effects. *Diode Lasers and Photonic Integrated Circuits*. 2012:247-333.

[42] Abdulrhmann S, Ahmed M, Yamada M. Influence of Nonlinear Gain and Nonradiative Recombination on the Quantum Noise in InGaAsP Semiconductor Lasers. *Optical Review*. 2002/11/01 2002;9(6):260-268. doi:10.1007/s10043-002-0260-4

[43] Mahmoud A, Ahmed M. Effect of asymmetric intermodal gain suppression on dynamics of multimode semiconductor lasers. *Optics Communications*. 2020/05/01/ 2020;462:125365. doi:https://doi.org/10.1016/j.optcom.2020.125365

[44] Petermann K. Longitudinal Mode Spectrum of Lasing Emission. In: Petermann K, ed. *Laser Diode Modulation and Noise*. Springer Netherlands; 1988:59-77.

[45] Al-Otaibi R, Ahmed M. Modelling of intensity noise, frequency noise and linewidth of semiconductor laser and their dependence on optical gain formulation. *Pramana*. 2021/08/19 2021;95(3):138. doi:10.1007/s12043-021-02164-3

[46] Agrawal G. Gain nonlinearities in semiconductor lasers: Theory and application to distributed feedback lasers. *IEEE Journal of Quantum Electronics*. 1987;23(6):860-868. doi:10.1109/JQE.1987.1073406

تحسين ليزر أشباه الموصلات ثابت الشدة للوصول لقدرات عالية في نطاق مئات الملي واط للاستخدام في التطبيقات الطبية: دراسة نظرية

فاطمة الشيخ، و **أبو بكر الزراد**، و **مصطفى أحمد**

قسم الفيزياء كلية العلوم، جامعة الملك عبد العزيز، جدة، المملكة العربية السعودية

المستخلص. ليزر أشباه الموصلات واعد للغاية في التطبيقات الطبية خاصة في العلاج الضوئي الديناميكي وهو نوع من العلاج الضوئي بالليزر. ويصنف ليزر أشباه الموصلات التقليدي المستخدم في هذا النوع من العلاج على أنه ليزر منخفض القدرة ينبعث منه إشعاع بقدرة في حدود عشرات الملي واط مما يتطلب رفع قدرة هذا الليزر لمئات الملي واط لتوسيع مجال تطبيقاته ليشمل تطبيقات طبية أخرى. تهدف هذه الدراسة النظرية إلى تعيين القيم المثلى لمعاملات ليزر أشباه الموصلات ثابت الشدة والتي تتحكم في خصائص منحنى تيار الضوء المميز وذلك نحو تحقيق كفاءة تدرج أعلى وقدرة خرج أعلى. تعتمد الدراسة على استخدام معادلات التغير الزمني لأعداد الفوتونات والالكترونات بنسخة الحالة المستقرة ومن ثم دراسة العلاقات بين كفاءة التدرج الكلي، والكفاءة الكمية التفاضلية، وعتبة التيار والقدرة المنبعثة. أشارت الحسابات إلى أنه يتم توقع قدرة في نطاق مئات الملي واط وذلك من خلال تصميم ليزر أشباه الموصلات ليكون تجويفه ذو وجه أمامي مضاد للانعكاس، ووجه خلفي عالي الانعكاس، وطول قصير مع معامل امتصاص منخفض لمادة الليزر ومعامل حصر ضوئي عالي. تتمثل نتيجة هذه الدراسة في تقديم نموذج لتصميم ليزر أشباه الموصلات عالي الطاقة لاستخدامه في العلاج الضوئي الديناميكي وفي تطبيقات طبية أخرى.

الكلمات المفتاحية: ليزر أشباه الموصلات، منحنى تيار الضوء، العلاج الضوئي الديناميكي، الكفاءة.